

Increasing Underwater Vehicle Autonomy by Reducing Energy Consumption

M. Chyba^a, T. Haberkorn^d, S.B. Singh^a, R.N. Smith^{b*}, S.K. Choi^c

University of Hawaii, Honolulu, HI 96822 USA

^aMathematics, College of Natural Sciences

^bOcean & Resources Engineering Department

^cAutonomous System Laboratory, College of Engineering

Université d'Orléans, 45067 Orléans Cedex 2, France

^dLaboratoire MAPMO

Abstract

In this paper, we concern ourselves with finding a control strategy that minimizes energy consumption along a trajectory connecting two given configurations. We develop an algorithm, based on our previous work with the time optimal problem, which provides implementable control strategies that are energy efficient. We find an interesting correlation between the duration of these trajectories and the optimal duration. We present the algorithm, control strategy and experimental results from our test-bed vehicle.

Key words: Autonomous Underwater Vehicle, Minimum Energy Consumption, Optimal Control, Experiments.

1 Introduction

Autonomous underwater vehicles (AUVs) are found to be essential to many underwater missions. Clearly, the onboard energy system is key to their ability to perform a prescribed mission. For a long duration mission, during which the AUV does not have the possibility to recharge, it is absolutely critical to take the energy demands of the vehicle into consideration. In this paper we address this question from a trajectory design point of view. Our goal is to design a control strategy that minimizes the energy consumption of the vehicle

* Corresponding author: ryan@ore.hawaii.edu, phone: (808) 956-9244, fax (808) 956-9139

along the path. The major difficulty is to produce control strategies that can be implemented onto a real vehicle. To this end, we develop an algorithm that takes thruster limitations into account. Interestingly, due to the physical features of the test-bed vehicle used for our experiments, and given a set of initial and final configurations, there exists a final time for which we realize the minimal consumption. For the set of configurations tested in this paper, this time is slightly more than 2.5 times the minimal duration of the trajectory. These trajectories can be theoretically computed, unfortunately they are not implementable onto a real vehicle due to multiple and rapid switching required by the thrusters. Our algorithm produces trajectories with a small number of actuator changes while still keeping energy consumption near optimal levels. These control strategies are implemented extremely successfully onto our test-bed vehicle. In this paper, we describe our experimental setting and results in detail.

2 Equations of Motion and Test-Bed Vehicle

The goal of this section is to derive the equations of motion for a controlled rigid body immersed in a real fluid and to introduce our test-bed vehicle used for the experiments. By real fluid, we mean a fluid which is viscous and incompressible with rotational flow.

2.1 Equations of motion

In the sequel, we identify the position and the orientation of a rigid body with an element of $SE(3)$: (b, R) . Here $b = (b_1, b_2, b_3)^t \in \mathbb{R}^3$ denotes the position vector of the body, and $R \in SO(3)$ is a rotation matrix describing the orientation of the body. The translational and angular velocities in the body-fixed frame are denoted by $\nu = (\nu_1, \nu_2, \nu_3)^t$ and $\Omega = (\Omega_1, \Omega_2, \Omega_3)^t$ respectively. Notice that our notation differs from the conventional notation used for marine vehicles. Usually the velocities in the body-fixed frame are denoted by (u, v, w) for translational motion (respectively surge, sway and heave) and by (p, q, r) for rotational motion (respectively roll, pitch and yaw), and the spatial position is taken as (x, y, z) . However, the chosen notation will prove more efficient, especially for the use of summation notation in our results.

We refer the reader to *Chyba et al. (2007) and (2008a)*, for the derivation of the general equations of motion for a submerged rigid body in a real fluid. In particular, in *Chyba et al. (2007)* we express the equations of motion as a forced affine-connection control system on the manifold $SE(3)$ to study the motion planning problem using kinematic motions. In the present paper, we

focus on designing and implementing efficient control strategies with respect to energy consumption onto our test-bed vehicle, hence we only repeat the assumptions related to our experimental set-up.

ASSUMPTION 2.1 *We take the origin of the body-fixed frame to be the center of gravity C_G . Moreover, we assume the body to have three planes of symmetry with body axes which coincide with the principal axes of inertia.*

Our assumptions on the geometry of the vehicle imply that the body inertia, added mass and moment of inertia matrices are all diagonal, and the added cross-terms are zero.

ASSUMPTION 2.2 *As in Chyba et al. (2008a) and (2008b), we make the following assumptions about the drag coefficients. We assume the drag force $D_\nu(\nu)$ and drag momentum $D_\Omega(\Omega)$ matrices are both diagonal. The contribution of these forces is quadratic in the velocities; $D_\nu^{ii}(\nu) = C_D \rho A |\nu_i| \nu_i$ where C_D (sphere) can be estimated as 1.2 for laminar flow and 0.2 for turbulent flow, ρ is the density of the fluid and A is the projected surface area of the object. With this assumption, the drag force and momentum are non-differentiable functions and theoretical analysis becomes difficult. To avoid difficulties, some restrict vehicle motion to a single direction, hence $|\nu_i| \nu_i = \nu_i^2$. We do not want to make this assumption because at least rotations are needed in both directions. Based on our test bed vehicle, our computations for the total drag force with respect to velocity suggests a cubic function with no quadratic or constant term as a good approximation. Thus, the contribution to the translational motions is given by $D_\nu(\nu) = \text{diag}(D_\nu^{i2} \nu_i^3 + D_\nu^{i1} \nu_i)$ and to the rotational motions by $D_\Omega(\Omega) = \text{diag}(D_\Omega^{i2} \Omega_i^3 + D_\Omega^{i1} \Omega_i)$ where D_ν^{ij} , D_Ω^{ij} are constant coefficients.*

Note that rotational viscous flow introduces fluid shear stresses which result in the addition of dissipative viscous drag. Due to the size, shape and operational velocity range of the test-bed AUV, pressure (form) drag is dominant and is the only drag force considered in the drag estimation in Assumption 2.2.

We also consider restoring forces moments. The only moment due to restoring forces is the righting moment $-r_B \times R^t(\rho g \mathcal{V} - mg)k$ where r_B is the vector from C_G to the center of buoyancy C_B , ρ is the fluid density, g the acceleration of gravity, \mathcal{V} the volume of fluid displaced by the rigid body and k the unit vector pointing in the direction of gravity.

DEFINITION 2.3 *Under our assumptions, the equations of motion, in the body-fixed frame, for a controlled rigid body submerged in a real fluid are given by:*

$$\begin{aligned} M\dot{\nu} &= M\nu \times \Omega + D_\nu(\nu)\nu + R^t(\rho g \mathcal{V} - mg)k + \varphi_\nu \\ J\dot{\Omega} &= J\Omega \times \Omega + M\nu \times \nu + D_\Omega(\Omega)\Omega - r_B \times R^t(\rho g \mathcal{V} - mg)k + \tau_\Omega \end{aligned} \quad (1)$$

where M accounts for the mass and added mass coefficients, J accounts for the body moments of inertia and added moments of inertia coefficients. The matrices $D_\nu(\nu)$, $D_\Omega(\Omega)$ represent the drag force and momentum. And, $\varphi_\nu = (\varphi_{\nu_1}, \varphi_{\nu_2}, \varphi_{\nu_3})^t$ and $\tau_\Omega = (\tau_{\Omega_1}, \tau_{\Omega_2}, \tau_{\Omega_3})^t$ account for the control forces.

In local coordinates, we have:

$$\dot{b}_1 = \nu_1 \cos \psi \cos \theta + \nu_2 R^{12} + \nu_3 R^{13}, \quad (2)$$

$$\dot{b}_2 = \nu_1 \sin \psi \cos \theta + \nu_2 R^{22} + \nu_3 R^{23}, \quad (3)$$

$$\dot{b}_3 = -\nu_1 \sin \theta + \nu_2 \cos \theta \sin \phi + \nu_3 \cos \theta \cos \phi, \quad (4)$$

$$\dot{\phi} = \Omega_1 + \Omega_2 \sin \phi \tan \theta + \Omega_3 \cos \phi \tan \theta, \quad (5)$$

$$\dot{\theta} = \Omega_2 \cos \phi - \Omega_3 \sin \phi, \quad (6)$$

$$\dot{\psi} = \frac{\sin \phi}{\cos \theta} \Omega_2 + \frac{\cos \phi}{\cos \theta} \Omega_3, \quad (7)$$

$$\dot{\nu}_1 = \frac{1}{m_1} [-(m_3)\nu_3\Omega_2 + (m_2)\nu_2\Omega_3 + D_\nu(\nu_1) - G \sin \theta + \varphi_{\nu_1}], \quad (8)$$

$$\dot{\nu}_2 = \frac{1}{m_2} [(m_3)\nu_3\Omega_1 - (m_1)\nu_1\Omega_3 + D_\nu(\nu_2) + G \cos \theta \sin \phi + \varphi_{\nu_2}], \quad (9)$$

$$\dot{\nu}_3 = \frac{1}{m_3} [-(m_2)\nu_2\Omega_1 + (m_1)\nu_1\Omega_2 + D_\nu(\nu_3) + G \cos \theta \cos \phi + \varphi_{\nu_3}], \quad (10)$$

$$\begin{aligned} \dot{\Omega}_1 = & \frac{1}{I_{b_1} + J_f^{\Omega_1}} [(I_{b_2} - I_{b_3} + J_f^{\Omega_2} - J_f^{\Omega_3})\Omega_2\Omega_3 + (M_f^{\nu_2} - M_f^{\nu_3})\nu_2\nu_3 \\ & + D_\Omega(\Omega_1) + \rho g \mathcal{V}(-y_B \cos \theta \cos \phi + z_B \cos \theta \sin \phi) + \tau_{\Omega_1}], \end{aligned} \quad (11)$$

$$\begin{aligned} \dot{\Omega}_2 = & \frac{1}{I_{b_2} + J_f^{\Omega_2}} [(I_{b_3} - I_{b_1} + J_f^{\Omega_3} - J_f^{\Omega_1})\Omega_1\Omega_3 + (M_f^{\nu_3} - M_f^{\nu_1})\nu_1\nu_3 \\ & + D_\Omega(\Omega_2) + \rho g \mathcal{V}(z_B \sin \theta + x_B \cos \theta \cos \phi) + \tau_{\Omega_2}], \end{aligned} \quad (12)$$

$$\begin{aligned} \dot{\Omega}_3 = & \frac{1}{I_{b_3} + J_f^{\Omega_3}} [(I_{b_1} - I_{b_2} + J_f^{\Omega_1} - J_f^{\Omega_2})\Omega_1\Omega_2 + (M_f^{\nu_1} - M_f^{\nu_2})\nu_1\nu_2 \\ & + D_\Omega(\Omega_3) + \rho g \mathcal{V}(-x_B \cos \theta \sin \phi - y_B \sin \theta) + \tau_{\Omega_3}], \end{aligned} \quad (13)$$

where $G = mg - \rho g \mathcal{V}$, $m_i = m + M_f^{\nu_i}$, $D_\nu(\nu_i) = D_\nu^{i2}\nu_i^3 + D_\nu^{i1}\nu_i$ and $D_\Omega(\Omega_i) = D_\Omega^{i2}\Omega_i^3 + D_\Omega^{i1}\Omega_i$.

In the equations of motion above, we assume that we have three forces acting at C_G along the three body-fixed axes and three pure torques about these three axes. This is unrealistic from a practical point of view and will be addressed as we present our test-bed vehicle in the next section. In the sequel, we will refer to these idealized controls as the six degree-of-freedom (6-DOF) controls.

2.2 Test Bed Vehicle

The test-bed vehicle used for our experiments is the Omni-Directional Intelligent Navigator (ODIN) shown in Figure 1. ODIN is owned and maintained by the Autonomous Systems Laboratory, College of Engineering at the University of Hawaii. A detailed description of ODIN can be found in *Chyba et al., (2008a and 2008b)*. From Figure 1, we clearly see that the forces from

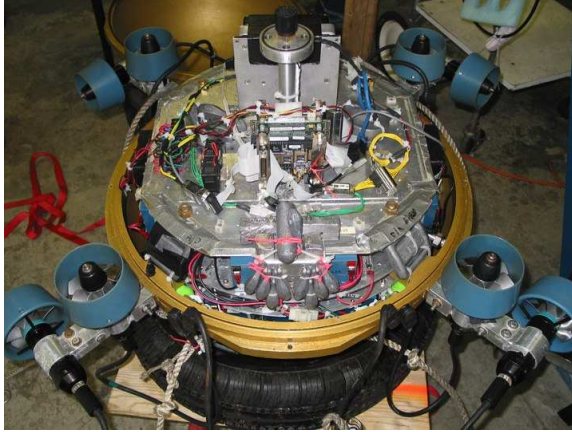


Fig. 1. *Omni-Directional Intelligent Navigator.*

the eight thrusters do not act directly at C_G . Control torques are obtained from the moments created by the applied forces. The consumption criterion in which we are interested is based upon the design and operation of the thrusters, which we will now examine in more detail. For implementation of control strategies, we must compute the transformation between the computed 6-DOF controls and the eight individual controls given to each thruster. We refer to the later as the eight dimensional thruster (8-DT) controls. First, let us denote γ_i , $i = 1, 3, 5, 7$ as the thrusts induced by the horizontal thrusters and γ_i , $i = 2, 4, 6, 8$ as the thrusts induced by the vertical thrusters. We assume that the points of application of the thrusts $\gamma_i^{(h,v)}$ lie in a plane which intersects the center of the spherical body of ODIN. By design, the distance from the center of the body-fixed reference frame (C_G) to C_B is small with respect to the radius of the sphere. This allows us assume that the actions of the thrusters can be decoupled. Hence, the horizontal thrusters contribute only to the forces φ_{ν_1} (surge) and φ_{ν_2} (sway) and to the torque τ_{Ω_3} (yaw). The vertical thrusters contribute only to the force φ_{ν_3} (heave) and to the torques τ_{Ω_1} (roll) and τ_{Ω_2} (pitch). Under these assumptions, we are able to determine that the linear transformation from the 6-DOF controls to the 8-DT controls is given by $TCM \cdot \gamma$ where $\gamma = (\gamma_1, \dots, \gamma_8)^t$. Here TCM stands for Thrust

Conversion Matrix, and is given by:

$$TCM = \begin{pmatrix} -e_1 & 0 & e_1 & 0 & e_1 & 0 & -e_1 & 0 \\ e_1 & 0 & e_1 & 0 & -e_1 & 0 & -e_1 & 0 \\ 0 & -1 & 0 & -1 & 0 & -1 & 0 & -1 \\ 0 & -e_3 & 0 & -e_3 & 0 & e_3 & 0 & e_3 \\ 0 & e_3 & 0 & -e_3 & 0 & -e_3 & 0 & e_3 \\ e_2 & 0 & -e_2 & 0 & e_2 & 0 & -e_2 & 0 \end{pmatrix} \quad (14)$$

for $e_1 = 0.7071$, $e_2 = 0.4816$ and $e_3 = -0.2699$.

On ODIN, the thrusters are independently powered and we can reasonably state that each thrust γ_i is bounded by fixed values:

$$\gamma \in \Gamma = \{\gamma \in \mathbb{R}^8 \mid \gamma^{\min} \leq \gamma_i \leq \gamma^{\max}, i = 1, \dots, 8\}. \quad (15)$$

Even though the min. and max. values vary with each thruster, we assume these bounds to be the same for each thruster: $\gamma^{\min} = -14.2791 \text{ N}$ and $\gamma^{\max} = 6.3925 \text{ N}$.

The numeric values used for the hydrodynamic parameters are given in Table 1. These values were derived from experiments performed on ODIN. The added mass and drag terms were estimated from formulas found in *Imlay (1961)*, *Allmendinger (1990)*. Moments of inertia were calculated using experiments outlined in *Bhattacharyya (1978)*. We used inclining experiments to locate and place C_B while we assume that C_G is located at the center of our body-fixed axis. The drag and C_B estimates were then adapted to match the experimental behavior of the vehicle.

m	126.55 kg	$\rho g \nabla$	1243.2 N	C_B	(0, 0, -7) mm
M_f^u	70 kg	M_f^v	70 kg	M_f^w	70 kg
I_x	5.46 kg.m ²	I_y	5.29 kg.m ²	I_z	5.72 kg.m ²
J_f^p	0 kg.m ²	J_f^q	0 kg.m ²	J_f^r	0 kg.m ²
D_ν^{11}	-27.03	D_ν^{21}	-27.03	D_ν^{31}	-27.03
D_ν^{12}	-897.66	D_ν^{22}	-897.66	D_ν^{32}	-897.66
D_Ω^{11}	-13.79	D_Ω^{21}	-13.79	D_Ω^{31}	-11.94
D_Ω^{12}	-6.46	D_Ω^{22}	-6.46	D_Ω^{32}	-6.94

Table 1
Hydrodynamic parameters.

3 Minimization Criteria and Maximum Principle

The main objective of this paper is to design control strategies that are efficient in terms of their energy consumption and time duration, and that can be implemented on our test-bed vehicle. The outline of our approach is as follows. Hereafter, all references to consumption will imply energy consumption of the vehicle. Given a set of initial (χ_0) and final (χ_f) configurations at rest (i.e. with zero velocities), we first use a direct method to numerically determine the optimal time to go from χ_0 to χ_f . Then, we consider the consumption minimum problem with a fixed time. This time is a multiple of the optimal time calculated earlier. Using a direct method again, we compute the consumption optimal strategy. Finally, we use similar techniques to those developed in *Chyba et al. (2008a and 2008b)* to produce consumption efficient trajectories (STP) that are implementable onto ODIN. Notice that the second step is necessary only to compare our implementable STP trajectories to the consumption minimal ones in order to assess their efficiency.

3.1 Criteria

Our ultimate goal is to minimize a combination of time and consumption. While the time is a notion that is uniquely defined, the consumption criterion is largely dependant on the considered mechanical system. The criterion we use in this paper is directly related to ODIN, and thus requires a detailed description.

Our test-bed AUV is powered solely by on board batteries, hence its autonomous abilities are directly related to the life-span of this power supply. By virtue of design, a time efficient trajectory will require a high level of consumption. With this in mind, it is an interesting question to determine how the energy consumption varies depending on the time duration of a given trajectory. This question is addressed in Section 3.2.2. For now, we focus on the consumption criterion for our specific vehicle. As discussed in Section 2.2, ODIN is controlled by eight external thrusters. These thrusters draw power from a bank of 20 batteries. All other on-board electronics such as the computer and sensors run on a separate bank of four batteries which supply enough power for ODIN to operate nearly indefinitely when compared to the life-span of the thruster batteries. Thus, minimizing energy consumption for a given trajectory directly corresponds to minimizing the amount of current pulled by the thrusters.

To this end, we set-up and performed a simple thruster calibration experiment. We supplied a known voltage function to each thruster which covered the

operational range of voltage inputs used during experiments. As the voltage changed, we continuously recorded the thrust output using a strain gauge, as well as the amps pulled by the thruster. Each thruster was tested four times through both positive and negative voltage ranges. The experimental data was then averaged over all tests and all thrusters to give the following simplified relation:

$$Amps(\gamma_i) = \begin{cases} -0.4433\gamma_i = \alpha_- \gamma_i, & \text{if } \gamma_i \leq 0 \\ 0.2561\gamma_i = \alpha_+ \gamma_i, & \text{if } \gamma_i \geq 0 \end{cases}, \quad (16)$$

where $Amps(\gamma_i)$ (A) is the current pulled when the thrust γ_i (N) is applied by the thruster. Since we know the relationship between input voltage and output thrust for each actuator from previous calibration experiments, we can estimate the consumption based on input voltage applied to the vehicle. Since all thrusters were designed to be identical and based on experimental data, we assume the same relation for all eight thrusters. Note that the relation is not symmetric. The thrusters have a preferred direction of thrust, which depending on the propeller's shaft design.

The lifespan of a battery is measured in $A.h$. Thus, we can write the consumption criterion of the eight thrusters as:

$$C(\gamma) = \int_0^T \sum_{i=1}^8 Amps(\gamma_i(t)) dt, \quad (17)$$

where the final time T can either be fixed *a priori* or remain as a free parameter in the optimization problem. If we choose to leave the final time as a free parameter, it is guaranteed to be finite. This is obvious since the batteries only hold a finite amount of energy, and whether ODIN reached the final destination or not, she cannot operate indefinitely. However, we do expect diminishing returns on a trajectory that lasts too long. The reason for this is that ODIN is slightly positively buoyant. Thus, we must expend energy just to keep her submerged. If the trajectory duration is too long, we will use all the battery power before the final configuration is reached. Thus, there exists a finite time after which any control strategy will spend more energy counterbalancing buoyancy rather than reaching the final configuration. Also, leaving the final time as a free parameter induces numerical difficulties in solving the optimal control problem simply by increasing the number of unknowns, among other issues. This fact and the above discussion lead us to determine and fix a finite final time for the trajectory and then optimize the energy consumption during this interval.

Since we can determine the minimum time T_{\min} to connect two terminal configurations, we have a lower bound on the trajectory duration. As mentioned earlier, this duration will clearly not be energy efficient. We begin by consid-

ering a fixed duration T , which is a multiple of T_{\min} :

$$T = c_T \cdot T_{\min}, \quad c_T \geq 1. \quad (18)$$

Note that the way we consider the problem, for $c_T = 1$ the solution of the minimum time and minimum consumption problems are the same. In Section 3.2.2, we examine the evolution of consumption as a function of c_T .

3.2 Maximum Principle

The maximum principle *Pontryagin et al. (1968)* gives necessary conditions for a control strategy and its corresponding trajectory to be optimal. While we will not use these conditions to design our implementable trajectories, it is important to discuss them to validate and discuss the solutions we obtain in Section 4 as well as to validate some of our numerical choices.

Let us introduce $\chi = (\eta, \nu, \Omega)$ and consider the optimal control problem that steers our AUV from an initial configuration χ_0 to a final configuration χ_T , while minimizing an integral criterion of the form $\int_0^T l(\chi(t), \gamma(t)) dt$, where $\gamma(t)$ is the 8-DT control. For instance, for the time minimization problem we have $l(\chi, \gamma) = 1$ and for the consumption minimization problem we have $l(\chi, \gamma) = \sum_{i=1}^8 \text{Amps}(\gamma_i)$ and $T = c_T T_{\min}$, $c_T \geq 1$.

To apply the maximum principle, we introduce the following Hamiltonian function H :

$$\begin{aligned} H(\chi, \lambda, \gamma) &= -\lambda_0 l(\chi, \gamma) + \lambda_\eta^t J(\eta) \nu \\ &+ \lambda_\nu^t M^{-1}(M\nu \times \Omega + D_\nu(\nu)\nu + R^t(\rho g \mathcal{V} - mg)k + \varphi_\nu) \\ &+ \lambda_\Omega^t J^{-1}(J\Omega \times \Omega + M\nu \times \nu + D_\Omega(\Omega)\Omega - r_B \times R^t(\rho g \mathcal{V} - mg)k + \tau_\Omega) \end{aligned} \quad (19)$$

where λ_0 is a constant that can be normalized to 0 or 1. Notice, for simplicity we express these equations with the 6-DOF control but for our minimization problems we will work with the 8-DT controls. The transformation between these two controls can be found in (14).

Assume there exists an admissible optimal control $\gamma : [0, T] \mapsto \Gamma$, such that the corresponding trajectory $\chi = (\eta, \nu, \Omega)$, solution of equations (2)-(13), steers the body from χ_0 to χ_T . Then, from the maximum principle there exists an absolutely continuous vector function $\lambda : [0, T] \mapsto \mathbb{R}^{12}$, $(\lambda, \lambda_0) \neq (0, 0)$, such that χ and λ are solutions almost everywhere (a.e.) on $[0, T]$ of:

$$\dot{\eta} = \frac{\partial H}{\partial \lambda_\eta}, \quad \dot{\nu} = \frac{\partial H}{\partial \lambda_\nu}, \quad \dot{\Omega} = \frac{\partial H}{\partial \lambda_\Omega}, \quad \dot{\lambda}_\eta = -\frac{\partial H}{\partial \eta}, \quad \dot{\lambda}_\nu = -\frac{\partial H}{\partial \nu}, \quad \dot{\lambda}_\Omega = -\frac{\partial H}{\partial \Omega} \quad (20)$$

and such that the maximum condition holds:

$$H(\chi(t), \lambda(t), \gamma(t)) = \sup_{u \in \Gamma} H(\chi(t), \lambda(t), u), \text{ a.e. on } [0, T]. \quad (21)$$

In the case where the final time T is a free parameter, we must add the condition $H(\chi(t), \lambda(t), \gamma(t)) = 0$. A triple (χ, λ, γ) that satisfies the maximum principle is called an extremal and $\lambda(\cdot)$ is called the adjoint vector. We define the functions κ_i , $i = 1, \dots, 8$, as the multiplying coefficient of γ_i in $H + \lambda_0 l(\chi, \gamma)$. The function κ_i is then the i^{th} component of the vector $(\lambda_\nu, \lambda_\Omega)^t TCM(M^{-1}, J^{-1})$. For instance:

$$\kappa_1 = -\frac{e_1 \lambda_{\nu_1}}{m_1} + \frac{e_1 \lambda_{\nu_2}}{m_2} + \frac{e_2 \lambda_{\Omega_3}}{I_{b_3} + J_f^{\Omega_3}}. \quad (22)$$

As we will see in the next two sections, these functions are critical to determine the structure of the extremals for our problem.

3.2.1 Time Minimization

Minimization of the final time has already been studied in previous papers such as in *Chyba et al. (2007 and 2008a)*. However, in these papers we consider the 6-DOF control $(\varphi_\nu, \tau_\Omega)$ as the real control, rather than the 8-DT control γ . Since our goal here is to minimize a combination of time and consumption, and because the consumption criterion is defined using the eight thrusters, we include a description of the time minimization problem for the 8-DT control.

Time minimization corresponds to the unit integral criterion $l(\chi, \gamma) = 1$. In this case, the maximum condition (21) implies that a time optimal control satisfies the following:

$$\gamma_i = \begin{cases} \gamma^{\min} & , \text{ if } \kappa_i < 0 \\ \in [\gamma^{\min}, \gamma^{\max}] & , \text{ if } \kappa_i = 0 \\ \gamma^{\max} & , \text{ if } \kappa_i > 0 \end{cases}, \quad i = 1, \dots, 8. \quad (23)$$

So, the zeros of κ_i determine the structure of the time optimal control. We call these functions the switching functions. The maximum principle implies that if $\kappa_i(t) \neq 0$ a.e. on $[0, T]$ the control γ_i takes its value in $\{\gamma^{\min}, \gamma^{\max}\}$ a.e. In this case, we say that γ_i is bang-bang. If there exist a nontrivial interval $[t_1, t_2] \subset [0, T]$ such that κ_i is identically zero on that interval, we say that γ_i is singular on $[t_1, t_2]$. Practically speaking, a thruster operating strictly at full power is usually driven by a bang-bang control, whereas a thruster operating at anything other than full power corresponds to a singular control. Finally, a switching time for γ_i is defined as a time for which γ_i is discontinuous; the

input command to the thruster is changed, or for which γ_i changes from bang to singular (or vice-versa).

In Figure 2 we represent a time optimal trajectory. The initial configuration is the origin and the final configuration is taken to be $\chi_T = (5, 4, 1, 0, \dots, 0)$. Both configurations are assumed to be at rest. To calculate this strategy, we use a direct method that discretizes the Optimal Control Problem (*OCP*) to transform it into a Nonlinear Programming Problem (*NLP*). The optimization variables of the (*NLP*) are the discretized state and control. To discretize the dynamic (2)-(13), we use a second order Runge-Kutta scheme. For the actual numerical solving, we use the *AMPL* modeling language *Fourer et al. (1993)* and *IpOpt Waechter and Biegler (2006)* nonlinear optimization code. The

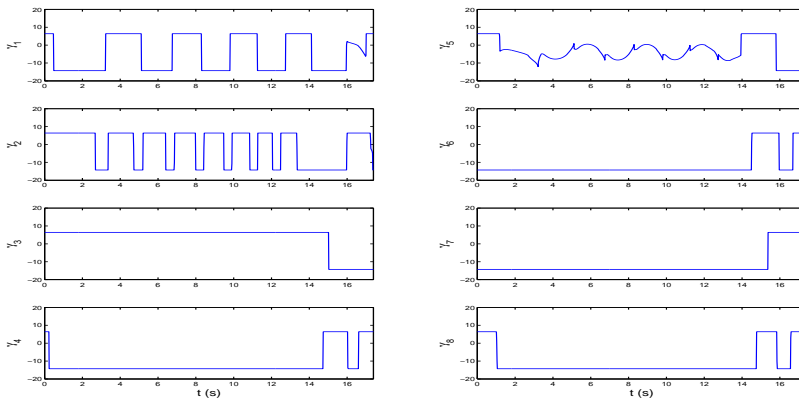


Fig. 2. *Minimum time control strategy for $\chi_T = (5, 4, 1, 0, \dots, 0)$.*

computed minimum time is $T_{\min} \approx 17.43$ s. As predicted by the maximum principle, the components of the 8-DT control are a concatenation of singular and bang-bang arcs.

3.2.2 Consumption minimization

In this case, we consider $l(\chi, \gamma) = \sum_{i=1}^8 Amps(\gamma_i)$. There is a crucial difference between this criterion and the previously discussed criterion for time minimization. Since the minimal time criterion does not depend on the controls, the normalization of the constant λ_0 does not influence the maximization condition of the Hamiltonian (trajectories corresponding to $\lambda_0 = 0$ are usually called abnormal). This is no longer true when considering the consumption criterion. A specific analysis needs to be conducted specifically for the case $\lambda_0 = 0$. But because our end goal of this paper is to produce implementable, consumption efficient trajectories, and the fact that our control strategy is developed using a switching time parametrisation algorithm not based on the maximum principle, we will omit this study here.

Let us consider the maximum condition when $\lambda_0 = 1$. The controls γ_i , for

$i = 1, \dots, 8$, are given by:

$$\gamma_i = \begin{cases} \gamma^{\min} & , \text{ if } \kappa_i < \alpha_- \\ \in [\gamma^{\min}, 0] & , \text{ if } \kappa_i = \alpha_- \\ 0 & , \text{ if } \kappa_i \in (\alpha_-, \alpha_+) \\ \in [0, \gamma^{\max}] & , \text{ if } \kappa_i = \alpha_+ \\ \gamma^{\max} & , \text{ if } \kappa_i > \alpha_+ \end{cases} \quad (24)$$

Here, if the function κ_i is not equal to α_- or α_+ on a nontrivial time interval, the corresponding γ_i will be piecewise constant and assumes the value γ^{\min} , 0 or γ^{\max} . If the switching function κ_i is identically equal to α_- (or to α_+) on a nontrivial time interval $[t_1, t_2]$ we say that γ_i is singular on $[t_1, t_2]$. A switching time is defined as before.

Before we provide a consumption minimal strategy and discuss its structure, we must rewrite our energy consumption criterion. Indeed, the direct method described in the previous section can be adapted to the minimum consumption problem. However, we need to take care as the criterion $C(\gamma)$ is not differentiable if one of the γ_i is zero (a situation that we do encounter since we impose both initial and final configurations to be at rest). To get around this, we decompose each γ_i into its negative (γ_i^-) and positive (γ_i^+) components. To this end, we define $\gamma_i^- = \min(\gamma_i, 0)$, $\gamma_i^+ = \max(\gamma_i, 0)$ and then $\gamma_i = \gamma_i^- + \gamma_i^+$, $\gamma_i^- \in [\gamma^{\min}, 0] = \Gamma^-$, $\gamma_i^+ \in [0, \gamma^{\max}] = \Gamma^+$. The consumption criterion can then be rewritten as:

$$C(\gamma) = \int_0^T \sum_{i=1}^8 \alpha_- \gamma_i^- + \alpha_+ \gamma_i^+ dt, \quad (25)$$

which is now \mathcal{C}^∞ with respect to γ_i^- and γ_i^+ . We are now able to apply our direct method as previously presented. Here we note that the above split criterion is equivalent to that given in (17) without requiring an additional constraint of the form $\gamma_i^-(t) \cdot \gamma_i^+(t) = 0$ a.e. on $[0, T]$. Suppose a pair of controls (γ^-, γ^+) do not satisfy this additional constraint. Then, there exists a pair of controls $(\tilde{\gamma}^-, \tilde{\gamma}^+)$ such that $\gamma^-(t) + \gamma^+(t) = \tilde{\gamma}^-(t) + \tilde{\gamma}^+(t)$ and $\tilde{\gamma}^-(t) \cdot \tilde{\gamma}^+(t) = 0$ a.e. on $[0, T]$. Clearly, $(\tilde{\gamma}^-, \tilde{\gamma}^+)$ yield a smaller consumption and thus (γ^-, γ^+) can not be optimal.

Now let us examine some results of applying the direct method to the criterion in (25). In Figure 3 we present three minimum control consumption strategies. Each of these strategies has the same initial and final configurations as in the time minimal section. The differences correspond to $c_T = 1.5, 2$ and 2.75 (we rescaled the final time to 1 in order to represent all three strategies on single graphs). Clearly, as we increase the final time, all thrusters use equal or less power throughout the duration of the motion (this is very evident in γ_3 and γ_6). Compare these three strategies to the minimum time strategy presented

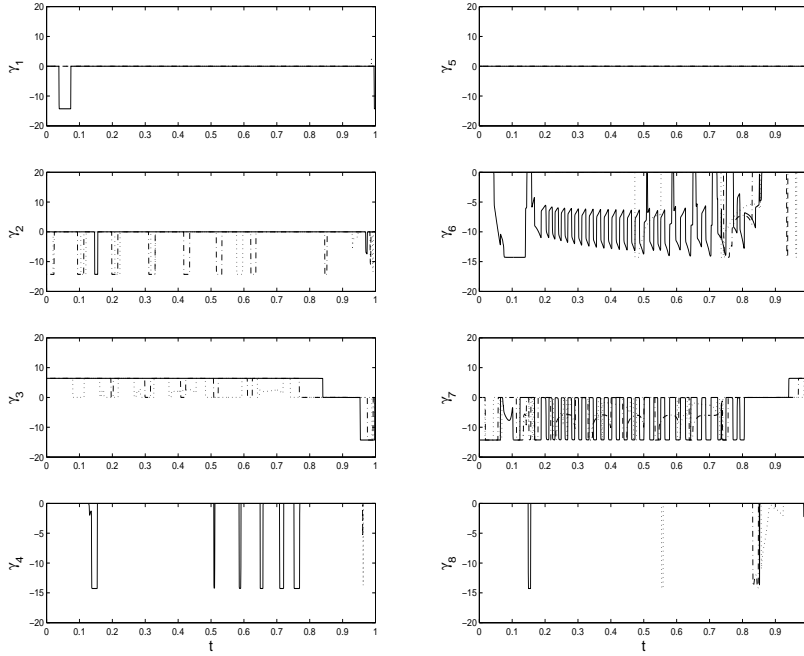


Fig. 3. Minimum consumption control strategies for $c_T = 1.5$ (plain), 2 (dashed), 2.75 (dotted) and for $\chi_T = (5, 4, 1, 0, \dots, 0)$.

in Figure 2. Note that the thrust control γ_5 is identically zero for consumption minimization (except for a small time interval at the end), while it is mainly singular and non-zero for the time minimum trajectory. Controls γ_3 and γ_7 are extensively used in both strategies. Considering their sign (mainly positive for γ_3 and negative for γ_7) as well as the TCM (14), we conclude that these 2 controls provide the surge and sway motion and a very minimal yaw torque. This was expected from our choice of initial and final configurations. Note that γ_6 is significant for $c_T = 1.5$, while it decreases $c_T = 2, 2.5$. This may indicate less of a need for roll and pitch evolution as the trajectory duration increases. This is expected based on strategies computed for the time minimum problem. Based on ODIN's thruster configuration and the final configuration considered (significantly more $b_{1,2}$ displacement than b_3), the time minimal strategy involved pointing the bottom of the vehicle at the destination and using the four vertical thrusters to realize the motion. In particular, moving as quickly as possible along the diagonal line connecting χ_0 and χ_T . As the duration increases the horizontal and vertical motions can be decoupled in a sense, allowing the horizontal thrusters to realize the horizontal displacement and the vertical thrusters to counteract buoyancy and realize the vertical motion. This is seen explicitly in Figure 4 which shows the evolution of η (position and orientation) corresponding to the control strategies of Figure 3. The major difference between the three trajectories lies in the roll and pitch evolution $\Omega_{1,2}$. Indeed, we see that for a final time close to the minimum one ($c_T = 1.5$) the overall inclination of the rigid body is much greater than when

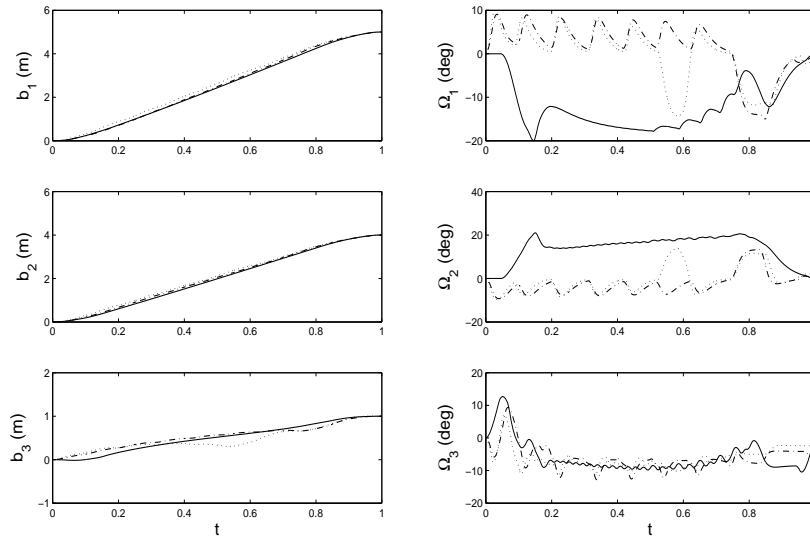


Fig. 4. Minimum consumption position/orientation evolution for $c_T = 1.5$ (plain), 2 (dashed), 2.75 (dotted) and for $\chi_T = (5, 4, 1, 0, \dots, 0)$.

the trajectory duration is lengthened. However, there is not much differences between the trajectories where $c_T = 2$ and $c_T = 2.75$. This can be explained by the fact that there is a much larger gain in consumption efficiency between $c_t = 1.5$ and $c_T = 2.0$ than between $c_t = 2.0$ and $c_T = 2.5$ (see Table 2).

The above figures and Table 2 prompts us to examine the relationship between c_T and consumption as mentioned before. Figure 5 shows the evolution of the consumption criterion when varying the duration of the final time (for the same initial and final configurations). By increasing the trajectory duration to

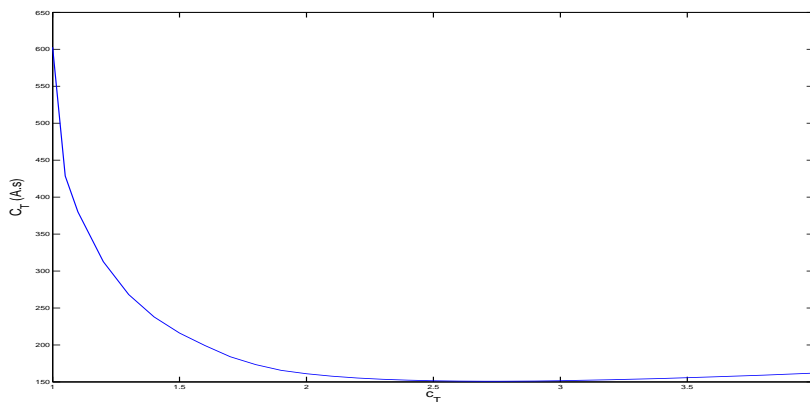


Fig. 5. Minimum consumption vs. c_T , for $\chi_T = (5, 4, 1, 0, \dots, 0)$.

roughly 2.5 times the time optimal duration, we can reduce the consumption by a factor of 4! It is interesting to note that the majority of this gain in efficiency is achieved for c_T close to 2. This is expected as a consequence from a previous remark on the existence of a finite trajectory duration which

realizes the optimal consumption. For this experimental set-up, Figure 5 gives a minimum consumption C^{\min} at $c_T^{\min} \approx 2.75$. Of course, c_T^{\min} will depend on the chosen set of hydrodynamic parameters as well as on the final configuration χ_T . Since a large majority of efficiency is achieved for small c_T , in practice we do not need to exactly compute the final time using c_T^{\min} . This further validates our choice of fixing T , rather than leaving it as a free optimization parameter, since the additional difficulties of leaving it free would only have given us the c_T^{\min} , without any information on the evolution of the criterion with respect to c_T .

Table 2 displays the minimum consumption for 4 distinct final configurations χ_T and 5 values of c_T near 2. The initial configuration is always taken to be the origin. All of the final configurations of Table 2 do not prescribe any

χ_T	$T^{\min}(s)$	C_1	$C_{1.50}$	$C_{2.0}$	$C_{2.5}$	C_{opt}
(5, 4, 1, 0, \dots , 0)	17.43	597.86	216.10	161.07	151.58	150.88
(3, 3, 3, 0, \dots , 0)	13.66	488.37	189.06	147.14	138.39	137.54
(5, 7, 0, \dots , 0)	22.22	753.53	273.53	196.61	184.12	182.92
(10, 8, 2, 0, \dots , 0)	31.48	1105.58	422.22	314.84	294.49	291.75

Table 2

Consumption for various χ_T and c_T .

inclination. This is not really a restriction since in practice we are more concerned with the displacement and can apply a rotation upon reaching the desired location. The computations presented in Table 2 show that we always reduce energy consumption significantly by allowing the trajectory duration to be greater than the optimal time. In particular, the all trajectory durations which achieved optimal consumption occurred for $c_T \in [2.75, 2.80]$. This strongly suggests that c_T^{opt} mainly depends on the hydrodynamic parameters (such as buoyancy) more than on the final configuration (if we prescribe final configurations with include no inclination). Studying such a dependence is not the aim of this paper but is of crucial importance when designing an underwater vehicle.

3.2.3 Remarks

From the maximum principle, the optimal trajectories for the consumption minimization with a fixed time are concatenations of piecewise constant and singular arcs. It is extremely difficult, if not impossible, to determine the switching times. We can even encounter a chattering control between a constant arc and a singular arc *Chyba and Haberkorn (2005)*. Clearly, the optimal consumption trajectories are not suitable for implementation onto ODIN as was previously seen in *Chyba et al. (2007 and 2008a)* when considering only

the time optimal strategy. For this reason we present a new algorithm to design trajectories that are consumption efficient and that can be implemented onto our test-bed vehicle.

4 Switching Time Parameterization for Consumption Criterion

From the analysis presented in the previous section and the information presented in Table 2, it is clear that the autonomy of our underwater vehicle can be dramatically improved by applying a minimum consumption thrust strategy (C_{opt}). The major problem is that such strategies cannot be implemented onto a test-bed vehicle due to their complicated structure, see Figure 3. For this reason, we must consider the design of consumption efficient thrust strategies which contain a small number of actuator switchings. To this end, we use a similar idea to that which was developed in *Chyba et al. (2008a)*: the so called Switching Time Parameterization Problem (*STPP*). To review, we rewrite the optimal control problem into a specific nonlinear programming problem for which the structure of the thrust strategy is imposed. We restrict our control set to the set of piecewise constant controls with only a small number of discontinuities representing the actuator switchings. Note that at a given discontinuity, several actuators are allowed to switch at the same time. Let p be the number of control discontinuities that we allow along the trajectory. Then, the new nonlinear programming problem is:

$$(STPP)_p \left\{ \begin{array}{l} \min_{z \in \mathcal{D}} \sum_{i=1}^p \sum_{j=1}^8 (\alpha_- \gamma_{j,i}^- + \alpha_+ \gamma_{j,i}^+) \\ t_0 = 0, t_{p+1} = T \\ t_{i+1} = t_i + \xi_i, i = 1, \dots, p \\ \chi_{i+1} = \chi_i + \int_{t_i}^{t_{i+1}} \dot{\chi}(t, \gamma_i^- + \gamma_i^+) dt \\ \chi_{p+1} = \chi T \\ z = (\xi_1, \dots, \xi_{p+1}, \gamma_1^-, \gamma_1^+, \dots, \gamma_{p+1}^-, \gamma_{p+1}^+) \\ \mathcal{D} = \mathbb{R}_+^{(p+1)} \times (\Gamma^- \times \Gamma^+)^{(p+1)} \end{array} \right. \quad (26)$$

where $\xi_i, i = 1, \dots, p+1$ are the time arclengths and $\gamma_i \in \mathcal{U}, i = 1, \dots, p+1$ are the values of the constant thrust arcs. $\dot{\chi}(t, \gamma_i^- + \gamma_i^+)$ is the right hand side of the dynamic system (2)-(13) with the constant control γ_i .

Note that a discontinuous control strategy is not implementable on our test-bed AUV since it could physically damage the thrusters. Hence, when initiating the solution of $(STPP)_p$ in $IpOpt$, we add linear junctions at the discontinuities of the control. This allows for a smooth and gradual transition from one control value to another so that the thruster will not be damaged by an

instantaneous change in prescribed thrust. The length of this junction is set to 1.2 seconds. To integrate the dynamic system of $(STPP)_p$ we use *DOP853*, a high order adaptive step integrator. This will give a better accuracy than a fixed step Runge-Kutta method. Note that this procedure is quite sensitive to the way in which we compute the gradient of the constraints (which is only the endpoint constraint since the final time constraint derivative is obvious) and to the initialization. Currently, we choose to use a simple finite difference method, but plan on moving to a variational approach. The variational approach has been delayed due to unfortunate complications caused by the additions of the linear junctions. Note that in the current solution method, we do find some local minima that occur very close to each other in terms of consumption efficiency and which are always feasible by the test-bed vehicle.

Table 3 summarizes consumption results for the $(STPP)_2$ and $(STPP)_3$ approach for final configurations identical to those used in Table 2 and with $c_T = 1.5, 2$ and 2.5 . Comparing this table to Table 2 we see that the con-

χ_T	$(STPP)_2$			$(STPP)_3$		
	$C_{1.5}$	C_2	$C_{2.5}$	$C_{1.5}$	C_2	$C_{2.5}$
$(5, 4, 1, 0, \dots, 0)$	228.43	163.89	150.64	228.72	164.91	157.51
$(3, 3, 3, 0, \dots, 0)$	221.53	155.56	148.45	205.79	155.09	146.17
$(5, 7, 0, \dots, 0)$	292.92	203.51	189.72	284.82	202.09	200.10
$(10, 8, 2, 0, \dots, 0)$	437.00	323.09		436.44	322.28	

Table 3
 $(STPP)_2$ and $(STPP)_3$ consumptions for various χ_T and c_T .

sumption calculated by the $(STPP)_2$ and $(STPP)_3$ approaches are of the same magnitude as seen previously. These values are exceptionally close to the optimal ones.

Figure 6 shows the computed thrust strategy corresponding to a $(STPP)_2$ solution with $c_T = 2$ and $\chi_T = (5, 4, 1, 0, \dots, 0)$. Contrary to the optimal thrust strategy, the one presented above is implementable onto a test-bed vehicle. There are only two times at which the actuators can switch during the trajectory, and moreover many of the controls are zero for an extended period of time. We use the following section to present experimental results of the implementation of the computed $(STPP)_2$ strategy onto the test-bed vehicle, ODIN.

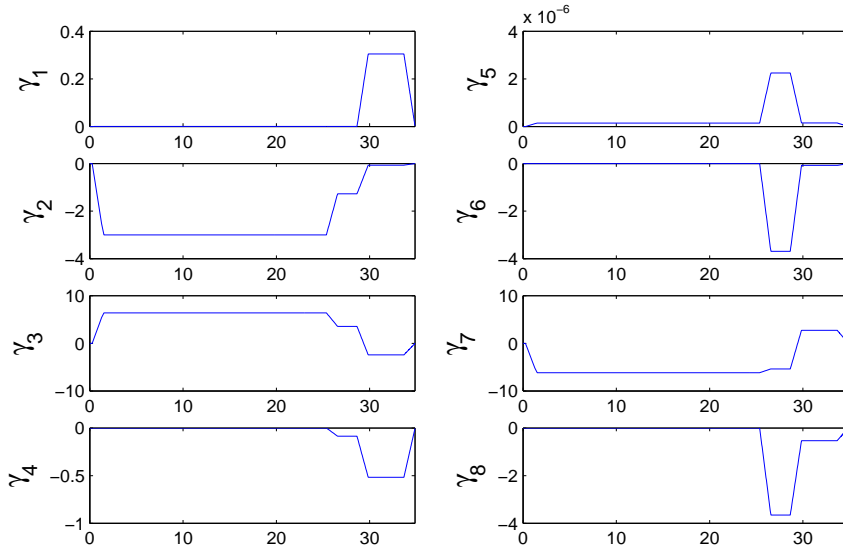


Fig. 6. $(STPP)_2$ thrust strategy for $c_T = 2$ and $\chi_T = (5, 4, 1, 0, \dots, 0)$.

5 Experiments

In an effort to validate extensions of geometric control theory and to bridge the gap between this theory and practical applications, we test our control strategies on the test-bed AUV ODIN described in Section 2.2. Here, we discuss the experimental set-up and highlight some advantages and limitations which we encounter. Weekly experiments are conducted in the diving well at the Duke Kahanamoku Aquatic Complex at the University of Hawaii. This diving well is a $25m \times 25m$ pool with a depth of $5m$. This controlled environment allows us to focus on particular aspects of each control strategy or to isolate model parameters without the influence of external disturbances such as waves, other vehicles and complex currents. The downside to such a facility is that conventional sonar systems generate too much noise to function as an effective and accurate positioning solution. More significantly, in the implementation of our efficient trajectories, ODIN is often required to achieve large ($> 15^\circ$) list angles which render the sonars useless for horizontal positioning. Also, the circulation pump creates a small magnetic field which affects the onboard compass.

Through the analysis of many experiments, we have been able to correct for the heading errors caused by the circulation pump. However, we have yet to implement an accurate and cost effective on-board positioning system. To resolve this issue, experiments are video taped from the 10m diving platform. This gives us a near nadir view of ODIN's movements. Videos are saved and horizontal position is post processed for later analysis. This solution is able to determine ODIN's relative position within the pool to less than $10cm$. However, closed-loop feedback on horizontal position is not possible. Since

our control strategies are directly based upon the vehicle model, this open loop framework does not hinder our implementation, and experimental results compare very well with theoretical predictions.

As noted throughout this paper, the control strategies we consider are for implementation onto an autonomous vehicle. For safety reasons, and in an effort to maximize the number of tests conducted each day, ODIN is tethered to the shore based command center. Even with this configuration, the strategies are run in autonomous mode, but real time data for orientation and depth are sent back to the operator throughout the experiment. Until recently, we have neglected the effects of the tether in the vehicle model. These effects were previously compensated through additional buoyancy and drag. Since we are confident that our base model for the vehicle is accurate, we can now fine tune the model by considering the effect of the tether.

The tether is a $\frac{3}{8}$ " Impulse *SP-C03* cable connected at the top of ODIN via a MOM-16-FS wet pluggable connector. The cable itself is negatively buoyant. In previous tests, foam was attached to the tether to make it positively buoyant. In this configuration, when ODIN is submerged, the tether rises vertically to the surface of the water and then lies on top of the water to the edge of the pool. Hence we incur additional buoyancy when ODIN dove as she pulled pieces of foam under the surface. When analyzing the consumption efficient strategies presented in this paper, we noticed large errors in the depth evolution which had not been seen for previously tested strategies. This is the main reason why we incorporate the tether study into this paper.

We considered six different configurations for the tether. Here, we only examine the two which displayed the best results and the original configuration for comparison. The considered configurations were chosen based on the movements ODIN needed to perform to realize our control strategies, the ease of implementation to the experimental procedure and the determination of the effect of the tether in a given configuration. The three configurations examined in this paper are:

- (C1) Remove all foam from the cable, attach the tether to the rear and bottom of ODIN and let the cable fall vertically downward to the bottom of the pool.
- (C2) Add foam to make the tether as neutrally buoyant as possible. Attach the tether to the rear of ODIN and have ODIN drag the tether behind her.
- (C3) Same as described before with the tether rising vertically from ODIN and lying atop the water's surface with added foam.

These three configurations are shown in Figure 7 to give a better understanding. For each configuration, we conducted experiments to determine which had the least effect upon the vehicle. This was done by comparing experimental

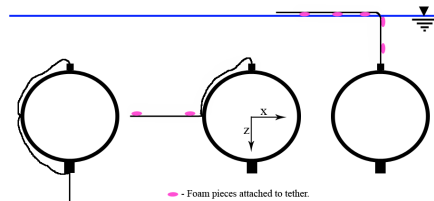


Fig. 7. The three examined tether configurations, from left to right $C1$, $C2$ and $C3$.

data for each configuration along a given trajectory to theoretical trajectories computed using the model which does not account for tether effects. The experimental data is the sensor data collected by ODIN (depth and orientation) and the $x - y$ position processed from the video recordings. We considered two separate theoretical trajectories for comparison. The pure theoretical trajectory is the evolution computed by feeding the model the theoretical thrust strategy as shown in Figure 6. This is the evolution we would expect if theory and experiment were one in the same. Obviously there are some uncertainties and unknowns which are uncontrollable and impossible to model accurately. One of these which we encounter is that ODIN does not apply the exact thrusts to the thrusters during the experiment. The reasons for this are outside the discussion here. Hence, we compare experimental evolutions to a more representative benchmark. Our theoretical trajectory is computed by feeding the model the actual thrusts applied by ODIN during the experiment. Thus, it is a post processed theoretical evolution. We can see the excellent correlation between the experimental data with the theoretical evolution in Figure 8, which validates the theoretical model. Even Figures 9 and 10 display good fits between the experimental and theoretical evolutions. In this section, we are concerned with the effects of the tether during testing and will now examine the presented data.

It was determined that configuration $C1$ (far left in Figure 7) had the least effect upon the vehicle's movement. The results of the separate tether con-

figurations are displayed in Figures 8, 9 and 10. Note the better correlation between experimental data and theoretical evolutions presented in Figure 8. Configuration C1 is now the current configuration used in the experimental set-up. Note that the experiments displayed in the figures correspond to the $STPP_2$ consumption efficient control strategy developed and presented in the previous sections.

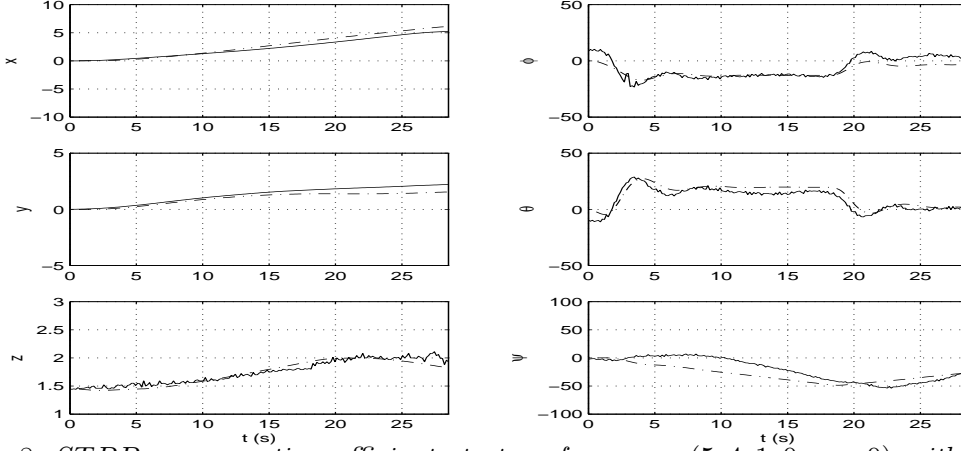


Fig. 8. $STPP_2$ consumption efficient strategy for $\chi_T = (5, 4, 1, 0, \dots, 0)$ with the tether in configuration C1. Theoretical (dash dot) and experimental (solid) evolutions are displayed.

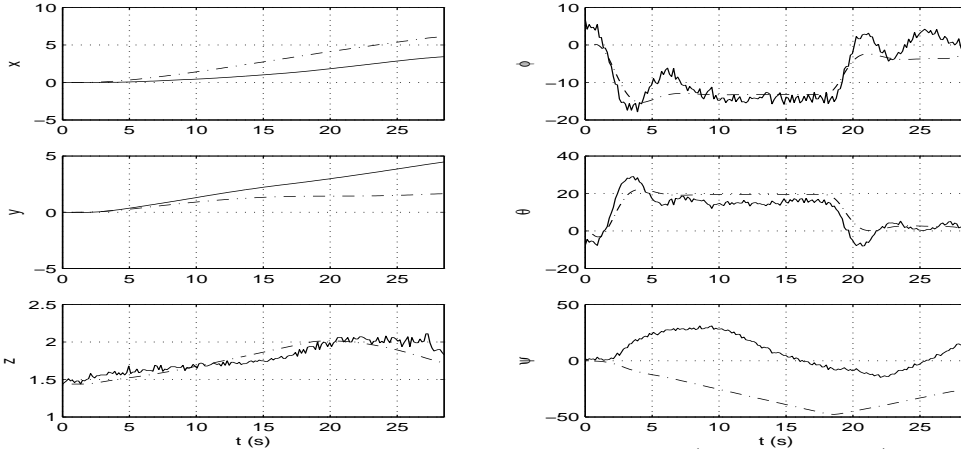


Fig. 9. $STPP_2$ consumption efficient strategy for $\chi_T = (5, 4, 1, 0, \dots, 0)$ with the tether in configuration C2. Theoretical (dash dot) and experimental (solid) evolutions are displayed.

From the point of view of the tether configuration, it is clear that tether configuration C1 yields the best overall fit for the given evolution. Similar results have been obtained for other motions as well. In Figures 9 and 10, note the greater discrepancies in horizontal evolution (x and y) from the evolution displayed in Figure 8. The difference between the tests for the evolution of ϕ and θ can be seen in the overshooting of the experimental trajectory when a large displacement is realized. Of most concern, for this study, is the fit of the evolution of z . The added buoyancy from the foam on the tether, which is not accounted for in the theoretical model, results in a poor correspondence

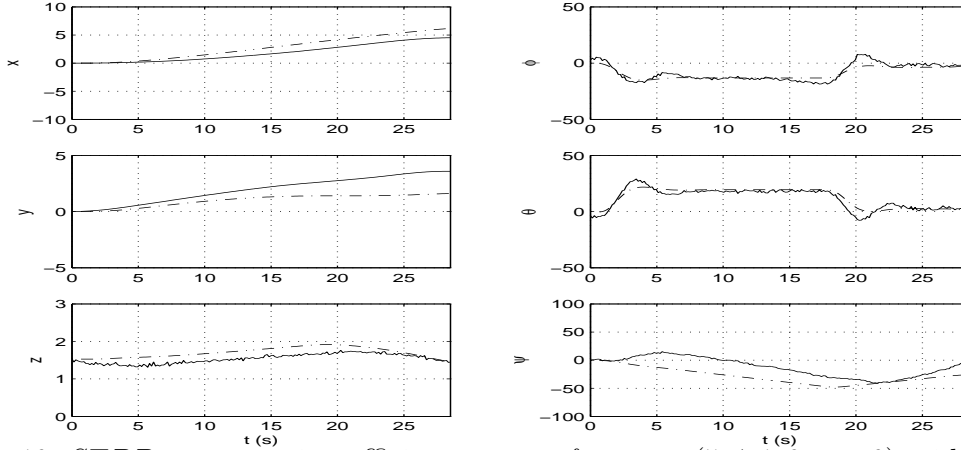


Fig. 10. $STPP_2$ consumption efficient strategy for $\chi_T = (5, 4, 1, 0, \dots, 0)$ with the tether in configuration C3. Theoretical (dash dot) and experimental (solid) evolutions are displayed.

between the experimental and theoretical evolutions. This may be a result from ODIN pulling more foam into the water which alters the buoyancy throughout the trajectory. Configuration C2 (Figure 9) has an acceptable fit, but notice that the low frequency oscillations of the depth evolution are exaggerated. Configuration C3 displays the worst correlation, and the experimental depth was consistently below the theoretical prediction. This is directly due to a greater buoyancy force than predicted by the model. Since the strategy is applied in fully open loop, there is no way for the vehicle to compensate for this. One advantage of tether configuration C1 is that the wetted surface of the cable remains constant for the duration of the trajectory, thus eliminating the need to compensate for changes in buoyancy during the motion. Also, the buoyancy is not being altered as more or less foam is under the surface. As for roll and pitch, the overshooting is probably a result of the added buoyancy from the foam and the inconsistency of the buoyancy force over the duration of the trajectory. Lastly, we note that the yaw (ψ) evolution does not match well with theoretical predictions for any configuration. This is due to the lack of external restoring forces and prominent drag forces acting on the spherical body in this degree of freedom. Again we remark that we are in full open loop and any parasite force from the horizontal thrusters results in a yaw displacement which cannot be corrected. Since the prescribed motion is mainly a horizontal displacement, and the horizontal thrusters are relied on more to generate this displacement (in comparison to the time minimal strategies, as noted in Section 3.2.2), we can not expect a good correspondence with the theory for yaw. Note here that the pure theoretical yaw evolution for the presented trajectory is identically zero for the entire duration. We clearly do not come close to this prediction since there must have been some parasite forces from transient thruster behavior. This can only be seen and compared by viewing the theoretical evolution created from the actual applied thrusts.

6 Conclusion and Future Tests

As seen in the previous section, as well in previous publications *Chyba et al.*, (2007 and 2008a), we have created a great theoretical model, and have obtained many excellent experimental results. We will continue to conduct weekly testing, including time and energy efficient strategy implementation. Along with this we will examine the effects of the tether in configuration C1 in more depth. This examination would lead to including a component in the the theoretical model which accounts for the effect of the tether. This will be examined from a numerical point of view as well as considering an actual theoretical term in the equations of motion. To further the examination of energy minimization, we are currently working on a method to monitor and record the actual energy consumption (in Amps) by ODIN over the duration of a given trajectory. This will allow us to compare experimental data with theoretical predictions regarding the actual energy used. Along with the time and energy efficient strategies we have presented, we are also working on designing control strategies for under-actuated vehicles. Not only is this interesting in its own right, but considering an under-actuated scenario may give insight into new energy minimizing control strategies.

References

- Allmendinger, E., 1990. Submersible Vehicle Design, SNAME.
- Bhattacharyya, R., 1978. Dynamics of Marine Vehicles, Wiley.
- Chyba, M. and Haberkorn, T., 2005. Autonomous Underwater Vehicles: Singular Extremals and Chattering. Proceedings of the 22nd IFIP TC 7 Conference on System Modeling and Optimization, Italy, 18-22 July 2005.
- Chyba, M., Haberkorn, T., Smith, R.N. and Wilkens, G.R., 2007. A Geometric Analysis of Trajectory Design for Underwater Vehicles, Discrete and Continuous Dynamical Systems-B. Submitted October 2007.
- Chyba, M., Haberkorn, T., Smith, R.N. and Choi, S.K., 2008a. Design and Implementation of Time Efficient Trajectories for an Underwater Vehicle, IEEE Journal of Ocean Engineering, Volume 35/1, pp. 63-76.
<http://dx.doi.org/10.1016/j.oceaneng.2007.07.007>
- Chyba, M., Haberkorn, T., Smith, R.N. and Choi, S.K., 2008b. Autonomous Underwater Vehicles: Development and Implementation of Time and Energy Efficient Trajectories, Ship Technology and Research, To appear 2008.
- Fourer, R., Gay, D.M. and Kernighan, B.W., 1993. AMPL: A Modeling Language for Mathematical Programming. Duxbury Press, Brooks-Cole Publishing Company.

Imlay, F.H., 1961. The Complete Expressions for Added Mass of a Rigid Body Moving in an Ideal Fluid. Technical Report DTMB, 1961.

Maurer, H., Büskens, C., Kim, J-H.R. and Kaya, I.C., 2005. Optimization Methods for Numerical Verification of Second Order Sufficient Conditions for Bang-Bang Controls. *Optimal Control Application and Methods*, 26:129-156.

Pontryagin, L.S., Boltyanski, B., Gamkrelidze, R. and Michtchenko, E., 1962. *The Mathematical Theory of Optimal Processes*. Interscience. New York.

Wächter, A. and Biegler, L.T., 2006. On the Implementation of an Interior-Point Filter-Line Search Algorithm for Large-Scale Nonlinear Programming. Research Report RC 23149, IBM T.J. Watson Research Center, Yorktown, New York.